Airborne laser scanning reveals large tree trunks on forest floor

Heinaro, Einari

2021-07-01

Heinaro , E , Tanhuanpaa , T , Yrttimaa , T , Holopainen , M & Vastaranta , M 2021 , ' Airborne laser scanning reveals large tree trunks on forest floor ' , Forest Ecology and Management , vol. 491 , 119225 . https://doi.org/10.1016/j.foreco.2021.119225

http://hdl.handle.net/10138/330351
https://doi.org/10.1016/j.foreco.2021.119225

Forest Ecology and Management 491 (2021) 119225

Contents lists available at ScienceDirect

Forest Ecology and Management

journal homepage: www.elsevier.com/locate/foreco

Airborne laser scanning reveals large tree trunks on forest floor

Einari Heinaro [a,*], Topi Tanhuanpää [a,b], Tuomas Yrttimaa [a,c], Markus Holopainen [a], Mikko Vastaranta [c]

[a] Department of Forest Sciences, University of Helsinki, P.O. Box 27 (Latokartankonkaari 7), 00014 University of Helsinki, Finland
[b] Department of Geographical and Historical Studies, University of Eastern Finland, P.O. Box 111, 80101 Joensuu, Finland
[c] School of Forest Sciences, University of Eastern Finland, P.O. Box 111, 80101 Joensuu, Finland

ARTICLE INFO

Keywords:
Airborne laser scanning
Light detection and ranging
Dead wood
Fallen trees
Biodiversity
Hough transform

ABSTRACT

Fallen trees decompose on the forest floor and create habitats for many species. Thus, mapping fallen trees allows identifying the most valuable areas regarding biodiversity, especially in boreal forests, enabling well-focused conservation and restoration actions. Airborne laser scanning (ALS) is capable of characterizing forests and the underlying topography. However, its potential for detecting and characterizing fallen trees under varying boreal forest conditions is not yet well understood. ALS-based fallen tree detection methods could improve our understanding regarding the spatiotemporal characteristics of dead wood over large landscapes. We developed and tested an automatic method for mapping individual fallen trees from an ALS point cloud with a point density of 15 points/m^2. The presented method detects fallen trees using iterative Hough line detection and delineates the trees around the detected lines using region growing. Furthermore, we conducted a detailed evaluation of how the performance of ALS-based fallen tree detection is impacted by characteristics of fallen trees and the structure of vegetation around them. The results of this study showed that large fallen trees can be detected with a high accuracy in old-growth forests. In contrast, the detection of fallen trees in young managed stands proved challenging. The presented method was able to detect 78% of the largest fallen trees (diameter at breast height, DBH > 300 mm), whereas 30% of all trees with a DBH over 100 mm were detected. The performance of the detection method was positively correlated with both the size of fallen trees and the size of living trees surrounding them. In contrast, the performance was negatively correlated with the amount of undergrowth, ground vegetation, and the state of decay of fallen trees. Especially undergrowth and ground vegetation impacted the performance negatively, as they covered some of the fallen trees and lead to false fallen tree detections. Based on the results of this study, ALS-based collection of fallen tree information should be focused on old-growth forests and mature managed forests, at least with the current operative point densities.

1. Introduction

The loss of biodiversity is a global challenge affected by climate change and the growing human population (Secretariat of the Convention on Biological Diversity, 2020). Sustaining biodiversity in the urbanizing world requires human actions. However, in order to focus these actions to the right places, there is a need for biodiversity-related information, such as knowledge of the locations of areas that are valuable regarding biodiversity.

Biodiversity is a complex concept that is often inspected at three levels: genetic level, species level, and ecosystem level (e.g., Secretariat of the Convention on Biological Diversity, 2005). The collection of detailed species-specific biodiversity information is very time-consuming and often limited resources require estimating biodiversity information using less detailed but more efficient methods. Such methods rely on indicators of biodiversity. In forest environment, biodiversity indicators are objects or features of forest structure that are easy to detect and can be used for estimating the biodiversity value of a certain area. Dead wood is one of the most important indicators of biodiversity in boreal forests, as it provides a habitat for a wide variety of species of which most are insects or fungi (Stokland et al., 2012). In addition to the species directly dependent on dead wood, there are numerous species that have an indirect dependence through other species (Jonsson et al., 2005). Dead wood can be roughly divided into downed dead wood, which consists of fallen tree trunks and branches lying on the forest floor, and standing dead wood, which includes

* Corresponding author.
E-mail address: einari.heinaro@helsinki.fi (E. Heinaro).

https://doi.org/10.1016/j.foreco.2021.119225
Received 13 January 2021; Received in revised form 25 March 2021; Accepted 30 March 2021
Available online 8 April 2021

standing dead trees and snags (e.g., Harmon et al., 1986). In this study, downed dead wood is determined as fallen trees lying horizontally on the forest floor.

Conventionally, dead wood has been mapped using sampling methods in which dead wood is inventoried from small areas (e.g., sample plots or strips) and these inventory data are used to estimate the distribution of the dead wood volume of a larger area (e.g., Ducey et al., 2013; Ståhl et al., 2001; Ståhl et al., 2010). Such sampling methods are rather time-consuming and enable only overall estimates of dead wood volumes. Furthermore, the occurrence of dead wood is often clustered, which limits the accuracy of field sampling -based dead wood volume estimates, especially if the sampling campaign has not had a specific focus on dead wood (Kangas, 2006). To overcome these challenges, remote sensing has been used to replace and supplement the laborious field-based dead wood mapping methods. Especially airborne laser scanning has been utilized, as it is able to characterize trees and the underlying topography simultaneously. ALS has been used to optimize dead wood field sampling locations by identifying typical dead wood hotspots, such as mature stands (Pesonen et al., 2010a, Pesonen et al., 2010b). Furthermore, dead wood volume has been modelled using the relationship between downed dead wood and ALS features describing low vegetation (Pesonen et al., 2008). Moreover, Miura & Jones (2010) derived ALS-based fractional metrics describing forest structure and found that the volume of downed dead wood was correlated with ALS metrics indicating gaps in canopy. The problem with such area-based approaches is that they observe dead wood indirectly using height- and intensity-based ALS features and observations of living trees. Especially in managed forests, the correlation between living and dead tree characteristics is rather low, which is rather problematic for approaches relying on the relationship between living and dead trees. In addition, the clustered occurrence of dead wood further limits the usefulness of coarse area-based approaches.

The recent development in laser scanning technology has enabled a shift from characterizing forests to the characterization of single trees and topography in detail. This shift has, in turn, enabled transforming from area-based approaches to direct measurements, which can potentially improve the accuracy of dead wood mapping significantly. Several studies have already inspected the potential of ALS for tree-level downed dead wood mapping. Blanchard et al. (2011) extracted downed log segments from rasterized ALS feature layers using image segmentation. Mücke et al. (2013) filtered a full-waveform ALS point cloud using filters based on normalized heights and echo width and created a rasterized height model from the remaining points. They then binarized this height model using a height threshold and extracted vectorized segments from the binary raster. Finally, fallen trees were identified from the vectorized segments by inspecting the area-perimeter-ratio and echo width variance of the segments. Lindberg et al. (2013) used template matching and dense ALS data for mapping individual fallen trees from a storm-damaged forest. The template matching procedure utilized both the point cloud and a rasterized height model derived from laser points located 0.2–1 m above ground. Similarly, Nyström et al. (2014) used template matching for detecting individual fallen trees from the same study area as Lindberg et al. (2013). However, they performed template matching on only a raster surface derived from single and last returns. Polewski et al. (2015) developed a multiphased method for detecting fallen trees. First, they extracted laser points located close to the ground and used point feature histograms (Rusu et al., 2008) to determine whether each point was a potential fallen tree point or not. Then, they generated fallen tree segment candidates by forming a line between each pair of potential fallen tree points located close to each other. The fallen tree segment candidates were filtered by inspecting the cardinality, distribution, and average fallen tree point probability of the points in the cylindrical neighborhood of each segment candidate. The remaining segment candidates were further filtered using 3D shape contexts (Frome et al., 2004) - a type of three-dimensional template - and a kernelized logistic regression classifier. Finally, the remaining segment candidates were merged using the normalized cut algorithm (Shi & Malik, 2000). Polewski et al. (2018) improved their method by considering segment-wise interactions when selecting fallen tree segment candidates.

The point density of the ALS data has a major impact on the detection of fallen trees. It affects the detection in at least two ways. Firstly, it determines how accurately the ground layer can be characterized. Less fallen trees are detected if laser returns originating from them are mistakenly classified as ground. In contrast, ground returns classified as above-ground returns may generate false detections. The level of detail with which the ground layer can be characterized is largely affected by the density of laser returns originating from ground. This density, in turn, is impacted by the point density of the ALS data as well as canopy cover, and the amount of shrubs and ground vegetation. Furthermore, the slope of the ground affects the accuracy of ground classification, as steep slopes hinder the detection of small height variations in the ground (e.g., Hodgson & Bresnahan, 2004; Su & Bork, 2006). In addition to the ground classification accuracy, the point density has a large impact on the number of laser returns originating from fallen trees. A small number of fallen tree returns makes it difficult to detect fallen trees, whereas a larger number of returns eases the detection.

The studies on ALS-based direct fallen tree detection conducted so far have lacked a comprehensive evaluation of the fallen tree characteristics as well as the vegetation structure characteristics that affect the performance of fallen tree detection. Furthermore, most studies have used ALS datasets with point densities that exceed the current densities used in large-scale laser scanning campaigns. Thus, the aim of this study was to develop and test an automated method for detecting individual fallen trees from an ALS point cloud with a moderate point density (15 points/m^2). Furthermore, the performance of the method was inspected in various types of forest and on various types of fallen trees. This paper aims to answer the following questions: How do the characteristics of fallen trees impact their detection? How does the structure of vegetation around the fallen trees impact their detection? Can fallen trees be mapped using moderate density ALS data? The detection method presented in this study relies on two-dimensional Hough transform -based line detection as well as classification based on machine learning. The hypothesis was that smaller details of objects are not visible in moderate density point clouds and object detection must rely on simplified shapes. Thus, a rather simple line detection approach was chosen as opposed to the more detailed approaches used by Lindberg et al. (2013), Nyström et al. (2014) and Polewski et al. (2015 & 2018). The detection method presented in this study was implemented with MATLAB (MathWorks Inc, Natick, Massachusetts, USA). The source code of the method is available as a Mendeley dataset (Heinaro, 2021a) and in GitHub (Heinaro, 2021b).

2. Material and methods

2.1. Study site

The study site covers a rectangular area of 16 km^2 in Hiidenportti National Park and its surrounding area in Eastern Finland (63.88°N, 29.15°E, Fig. 1). The area represents typical boreal forest conditions dominated by Norway spruce (*Picea abies L. Karst*), Scots pine (*Pinus sylvestris*), silver birch (*Betula pendula*), and downy birch (*Betula pubescens*). Also scattered European aspens (*Populus tremula*) are met in western and eastern parts. These parts of the study site are conservation areas characterized by old-growth forest. The central part of the study site consists of state-owned forests, some of which are intensively managed. The elevation of the study site varies between 190 and 250 m above sea level.

2.2. Reference data

The field reference data consist of 273 fallen trees measured on 103

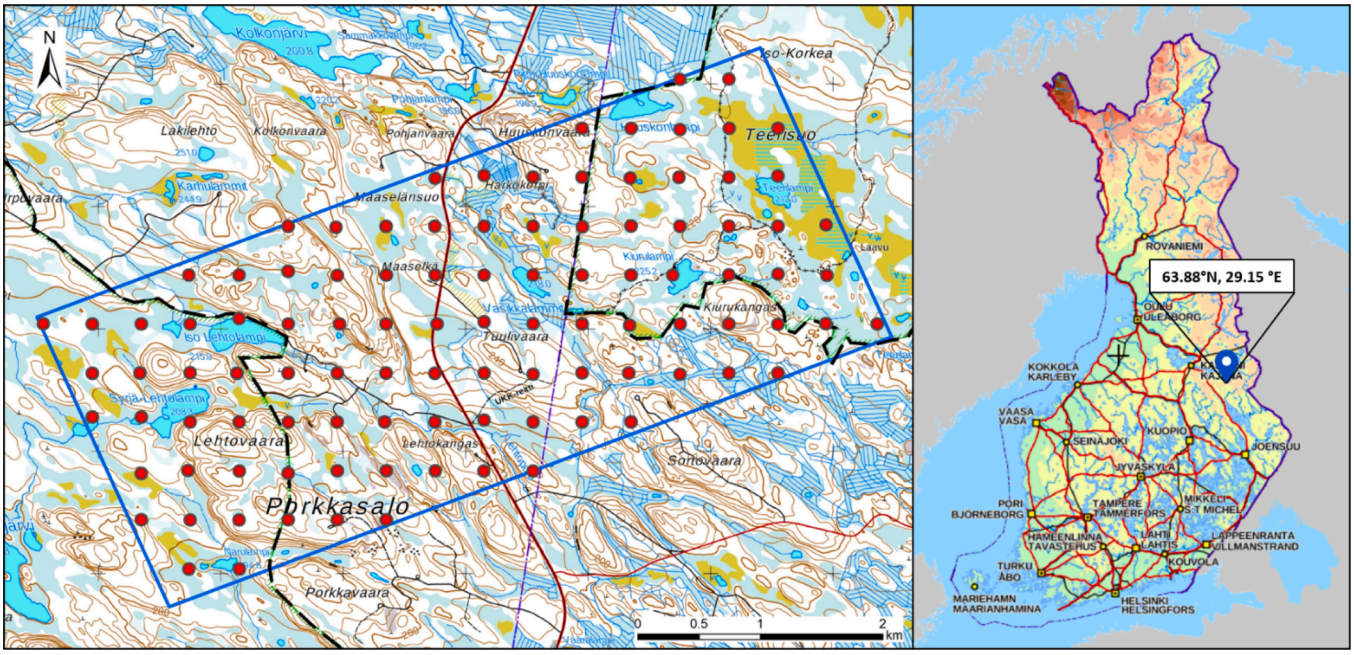

Fig. 1. The location of the study site and the distribution of sample plots. The rectangular area shows the bounds of the study site while the locations of sample plots are marked with circles. The region to the west of the western dashed line is Hiidenportti National Park and the region to the east of the eastern dashed line is Teerisuo-Lososuo conservation area. The region between the dashed lines is state-owned forest. (Background maps: National Land Survey of Finland).

circular sample plots that were selected with systematic sampling (Fig. 1) to ensure a representative sample of the study area. The distance between neighboring sample plots was approximately 400 m in cardinal directions. In case a sample plot happened to be placed at the border of two forest stands, the location of the sample plot was slightly adjusted to fully represent only a single forest stand. The radius of each sample plot was 9 m. A total number of 86 sample plots were located in old-growth forest and 17 sample plots were located in managed forest.

The field inventory data were collected between July and September 2019. Locations of the fallen trees were determined by measuring the position of both ends of the trees with a Trimble R2 (Trimble Inc., Sunnyvale, California, USA) real-time kinematic global navigation satellite system (GNSS). All fallen trees that were even partially located within the sample plots were measured in full considering a minimum diameter threshold of 100 mm. The lengths of the fallen trees were determined from the GNSS measurements and the diameters of the fallen trees were measured using steel calipers. The diameter was measured at a 1.3-meter distance from the bottom-end of the fallen tree, thus representing the diameter at breast height (DBH). In case the breast height could not be determined, the diameter was measured at the base of the fallen tree. The tree species was determined based on visual interpretation. The volume of the fallen trees was estimated with species-specific, nationwide volume equations (Laasasenaho, 1982) where DBH and length were used as explanatory variables. The state of decay was determined by following the guidelines of Finnish national forest inventory (see Appendix A). Silver birch and downy birch were handled as a single species class. Table 1 presents a summary of the attributes of the field-measured fallen trees. Table 2 shows how the fallen tree attributes differed between the managed forest and old-growth forest plots, whereas Table 3 presents the difference in attributes between sample plots with different prominent living tree species. The prominent tree species of each sample plot was determined as the species with the largest total volume.

In addition to the fallen trees, all living trees with a DBH over 45 mm within the sample plots were measured to describe the forest characteristics of each sample plot. The locations of the living trees were determined by measuring the direction and distance from the sample plot center. In addition, the DBH and species were recorded for all trees

Table 1
Summary of the attributes of the field-measured fallen trees.

	Total	Scots pine	Norway spruce	Silver and downy birch	Aspen
Number of trees	273	84	148	37	4
Decay class					
Min	1	1	1	1	3
Median	2	1	2	2	4.5
Mode	1	1	2	1	5
Max	5	5	5	5	5
Diameter (mm)					
Min	100	100	100	103	180
Mean	176.3	161.6	180.8	176.5	318.8
Max	450	297	401	363	450
Standard deviation	60.4	48.3	61.2	52.7	97.9
Length (m)					
Min	1.5	1.5	1.6	1.9	5.9
Mean	10.7	9.4	12	9.1	7.7
Max	23.1	22.1	23.1	21.2	12.1
Standard deviation	4.9	4.4	4.8	5.1	2.6
Volume (m^3)					
Min	0	0	0	0.007	0.032
Mean	0.134	0.098	0.155	0.085	0.459
Max	1.015	0.668	1.015	0.467	0.706
Standard deviation	0.178	0.132	0.199	0.082	0.268

Table 2
Summary statistics of the attributes of the field-measured fallen trees in managed and old-growth forests.

	Managed forest	Old-growth forest
Most frequent species	Scots pine	Norway spruce
Median decay class	1	2
Mean diameter (mm)	150.8	177.8
Mean length (m)	7.2	11.2
Mean volume (m^3)	0.06	0.14

Table 3
Summary statistics of the attributes of the field-measured fallen trees in pine-, spruce-, and birch-dominant sample plots.

Prominent species	Scots pine	Norway spruce	Silver and downy birch
Most frequent species	Scots pine	Norway spruce	Scots pine
Median decay class	2	2	1
Mean diameter (mm)	163.2	189.1	134.1
Mean length (m)	9.6	11.6	9.3
Mean volume (m^3)	0.091	0.170	0.035

(i.e., tally trees). Furthermore, several trees from each represented species at each sample plot were selected as sample trees whose heights were measured. The trees were selected visually, ensuring that the sample trees were a representative sample of all trees within the sample plot. The allometric relationship between the DBH and height of the sample trees was then used to estimate the heights of the tally trees. Näslund's (1936) function was used for this estimation. The undergrowth of each sample plot was characterized by counting the species-specific number of trees and shrubs with a DBH under 45 mm and a height over 1.3 m from a sample plot with a 5.4-meter radius.

Several stand characteristics were calculated for each sample plot using the measured attributes of tally trees and undergrowth within each sample plot, as well as the properties of the ALS data (Appendix B). The stand characteristics were aggregated from individual tree attributes either using sum or weighted mean. All stand characteristics, apart from canopy cover, were estimated using the field-collected data. The canopy cover was calculated from the ALS data using the same method as Polewski et al. (2015) where canopy cover was determined as the proportion of grid cells (cell size 0.5 m) within the sample plot that contained laser points above 5 m from ground. Median stand characteristics of the managed and old-growth forest plots are presented in Appendix C, and the relationship between most of the stand characteristics and the amount of undergrowth is presented in Appendix D.

2.3. Airborne laser scanning data

The airborne laser scanning (ALS) data were collected on May 17th, 2019 using a Riegl VQ1560i laser scanner (RIEGL Laser Measurement Systems GmbH, Horn, Austria). The flying altitude and scan angle were 1000 m and 40°, respectively, resulting in a swath width of 728 m and a laser footprint of 25 cm. The data were collected using five parallel flight lines (strip overlap 30%) and one flight line perpendicular to the other lines. The point density of the data was approximately 15 points/m^2, although in the areas covered by more than one strip the point density was significantly higher. The data were collected in leaf-off conditions just after the spring snowmelt to maximize the visibility of below-canopy objects such as fallen trees.

2.4. Pre-processing

The ALS data were classified into ground and above-ground points using Terrascan software (Terrasolid Ltd., Espoo, Finland). The ground points were extracted using a ground classification algorithm similar to the one presented by Axelsson (2000). The ground points were used for creating a digital terrain model (DTM). The above-ground points were normalized by subtracting the corresponding DTM value from the height values of each above-ground point. Finally, only the points within the height range between 0.2 and 1 m above ground were extracted for further processing based on the presumed occurrence of fallen trees as suggested by Yrttimaa et al. (2019).

2.5. Filtering the point cloud

Some of the laser points located in the 0.2–1-meter height range originate from fallen trees. However, a large proportion of the points originate from other sources, such as boulders, shrubs and small understory trees. The latter points need to be removed, so that they are not mistakenly classified as fallen trees. A filtering algorithm was created for this task. The algorithm was based on the observation that fallen trees are line-like objects, whereas other objects close to the ground are more irregularly shaped. Thus, the points originating from objects other than fallen trees can be removed by inspecting the shapes of groups of points in the point cloud. The filtering algorithm works as follows:

1. The points are projected onto the xy-plane.
2. A binary image of the point cloud is created by placing a grid on top of the point cloud. Each grid cell with points inside is assigned the value 1. Other grid cells are assigned the value 0. A cell size of 0.2 m was used in this study.
3. The binary image is segmented into connected components. Connected components consist of grid cells with the value 1 that are in the 8-neighborhood of each other.
4. Shape descriptors are calculated for each connected component. The shape descriptors describe a certain geometrical property of the connected component, such as the area, perimeter or circularity of the component.
5. The connected components are classified as belonging or not belonging to fallen trees using a statistical classifier. A shallow neural network was used as the classifier. The neural network was trained with a training set of connected components that were labeled manually.
6. The points are extracted that are located within the connected components that were labeled as belonging to fallen trees.

2.6. Line detection based on Hough transform

After running the filtering algorithm on the point cloud, the remaining laser points should mostly originate from fallen trees. Thus, the next step was to detect the fallen trees from the point cloud. Fallen trees are line-like objects and thus the fallen trees can be detected using a line detection algorithm. To simplify the detection, the remaining laser points were first projected onto the xy-plane to enable two-dimensional (2D) line detection. Then, a grid with a cell size of 20 m was set on top of the point cloud and the points were grouped based on the grid cell within which they were located. This enabled inspecting each grid cell separately, which in turn reduced the computational cost of the algorithm. After grouping the points, initial fallen tree segments within each grid cell were detected using an iterative Hough transform -based line detection algorithm inspired by the method presented by Dalitz et al. (2017). The Hough transform (Duda & Hart, 1972; Hough, 1962) detects lines by transforming points into lines/curves in the parameter space and finding the intersection of these lines/curves. The coordinates of this intersection in the parameter space are the parameters of the best-fit line of the points. To enable the detection of several lines in a single grid cell, the points forming an already detected line must be removed, as otherwise running the Hough transform again would result in the same line parameters. Thus, the iterative Hough transform consists of two steps that are run iteratively: finding the parameters of the best-fit line using Hough transform and removing the points that are within a certain distance from this line. The distance threshold was set to 0.5 m. This process is stopped once a stopping condition is met. In this study, the iterative line detection was stopped once four points or less were located within 0.5 m from the most recently detected line.

The parameters received as output from the Hough transform describe a line bounded by the borders of the grid cell within which the line was detected. However, the true bounds of a fallen tree are likely somewhere else than at the borders of the grid cell. Thus, the detected lines must be cut into line segments that represent the fallen trees (Fig. 2a–d). This was done by finding the laser points close to each detected line (within 0.5 m from the line) (Fig. 2b), projecting these points onto the line (Fig. 2c) and finding discontinuities along the line.

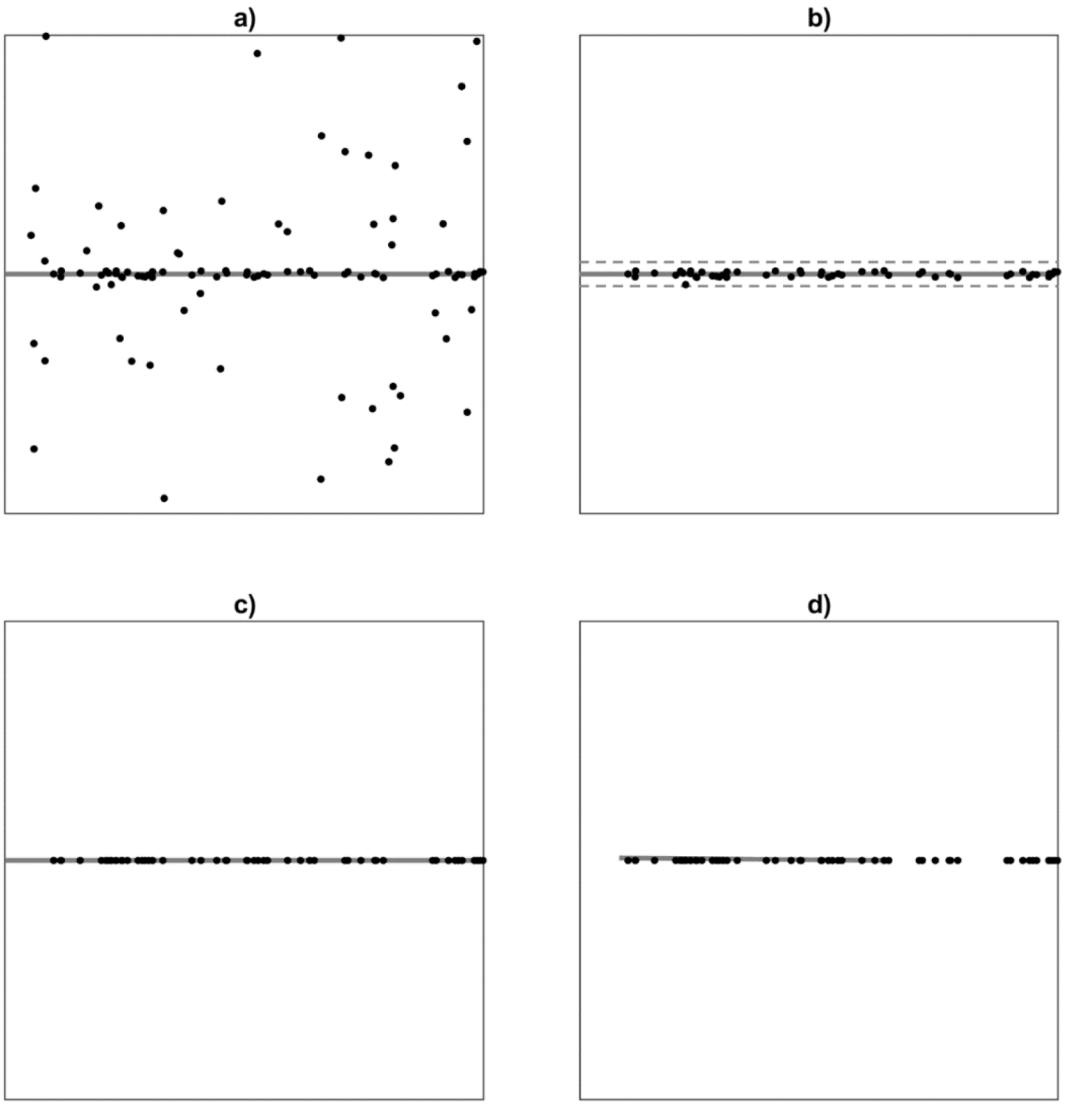

Fig. 2. Forming a line segment. a) A line has been detected from the point cloud. At this stage, however, the end points of the line are at the borders of the grid cell within which it was detected. b) The points located close to the detected line are extracted. The dashed lines depict the threshold distance to the detected line. c) The points close to the line are projected onto the line. Several discontinuous point groups can be identified from the projected points. d) The line segment is formed to the location of the largest point group.

The discontinuities were found by inspecting the distances between each adjacent projected point along the line. If the distance between two adjacent points was over 1 m, a discontinuity was identified and the points before and after this discontinuity were assigned to separate groups. A line segment was formed only from the largest group of points along the line (Fig. 2d). The end points of the line segment were defined as the first and last projected point in the group.

As the initial line segments were delineated for each grid cell separately, there were situations where trees crossing the borders of grid cells were represented by more than one line segment. Thus, the next step in the line detection process was to merge line segments originating from the same tree. This was done by inspecting all delineated line segments and merging the segments based on three criteria. Two line segments were merged if:

1. The difference between the slopes of the line segments was less than 5°.
2. The distance between one end of the first line segment and one end of the second line segment was less than 2 m.
3. The overlap percentage of the line segments was less than 10%. The overlap percentage was calculated by first projecting the line segments onto the × or y axis depending on which direction the rate of change of the longer line segment was larger. Then, the overlap percentage was determined by dividing the length of the section where the projected line segments overlap with the length of the shorter projected line.

2.7. Extracting point cloud representations of fallen trees

The line detection algorithm introduced in Section 2.6 delineated line segment representations of fallen trees. These line segments can be used for estimating the length of the fallen trees and calculating the number of fallen trees within a certain area. However, in order to enable estimating other fallen tree attributes, such as the DBH or volume, the laser points originating from each fallen tree need to be extracted. Further in the text, the term ‘line segment’ refers to a line-like representation of a fallen tree (i.e., a line bounded by two end points). The term ‘point cloud representation’ refers to a group of points in the ALS point cloud representing an individual fallen tree. The term ‘fallen tree

segment' refers to a fallen tree detected from the point cloud in general (i.e., the combination of both the line segment and point cloud representation of an individual fallen tree).

Point cloud representations of fallen trees were extracted using a region growing algorithm. The region growing algorithm grew the fallen trees around their line segment representations in the following way:

1. The line segments were first sorted into descending order based on their length (Fig. 3a).
2. Starting from the longest line segment (Fig. 3b):
   a. The points whose distance to the line segment was smaller than 0.5 m were assigned to a group of points representing an individual fallen tree (Fig. 3c).
   b. Additional points were added to the group in an iterative manner if their distance to any point already assigned to the group was less than 0.2 m (Fig. 3d).
   c. After no additional points were found, the points assigned to the group were removed from the point cloud and the region growing algorithm was repeated with the next longest line segment.

The point cloud representations of fallen trees allow estimating additional parameters, such as the tree diameter, that can be used together with the length of the line segment representation to estimate the volume of the fallen tree. Furthermore, the point cloud representations of fallen trees can be input into a classifier that detects whether the point cloud representation really represents a fallen tree or something else.

2.8. Final classification

The final step of the fallen tree detection process was to classify each detected fallen tree segment as a true or false fallen tree segment. This step was necessary, as the parameters of the iterative Hough line detection were selected so that the method rather overdetected than underdetected lines, i.e., the method was more likely to generate false fallen tree detections than to miss a true fallen tree. A convolutional neural network (CNN) was used for classifying the point cloud representations of the segments. In order to enable using a pretrained CNN, the point cloud representations were transformed in the following way:

1. The points belonging to a fallen tree segment (Fig. 4a) were rotated. The angle of rotation was determined by the angle between the y-axis and the line segment representation of the fallen tree segment. Thus, after the rotation, the fallen tree segment lay on the y-axis (Fig. 4b).
2. The rotated points were transformed into a binary image (cell size 0.2 m) in which each cell contained the value one if some points fell within it and the value zero otherwise.
3. The binary image was scaled and padded so that the image size matched the input image size of the CNN (Fig. 4c).

A pretrained CNN was used for the task of classifying true and false fallen tree segments. The pretrained network was tuned using training data of 3816 manually classified point cloud representations of fallen trees, of which 70% were used for training and 30% for validation. The manually classified data were collected by extracting the point clouds from 100 circular test sites (radius 35 m) distributed systematically across the study area, running the iterative line detection (Section 2.6)

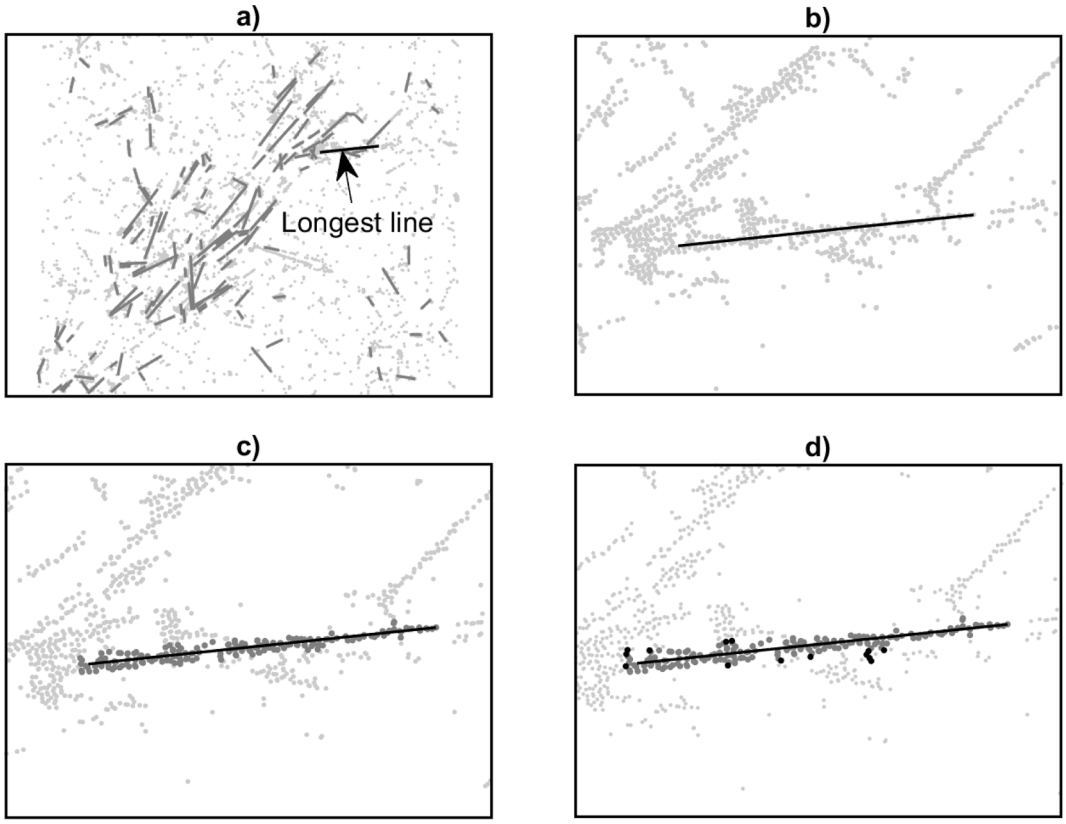

Fig. 3. Extracting the points belonging to a fallen tree. a) Line segments have been detected from the point cloud using iterative Hough transform. The light gray dots are laser points, and the lines are detected line segments. The black line is the longest line segment, which will be processed first. b) A close-up view of the longest line segment. No point grouping has been performed yet. c) Points within 0.5 m from the line segment are assigned to the same group representing an individual fallen tree. The darker gray dots represent the grouped points. d) More points are added to the group iteratively. A point is added to the group if its distance to any point already assigned to the group is less than 0.2 m. The dark gray dots are the previously grouped points, whereas the black points are the new points assigned to the group. After this step, the points assigned to the group are removed from the point cloud, and the whole process is repeated for the next longest line segment.

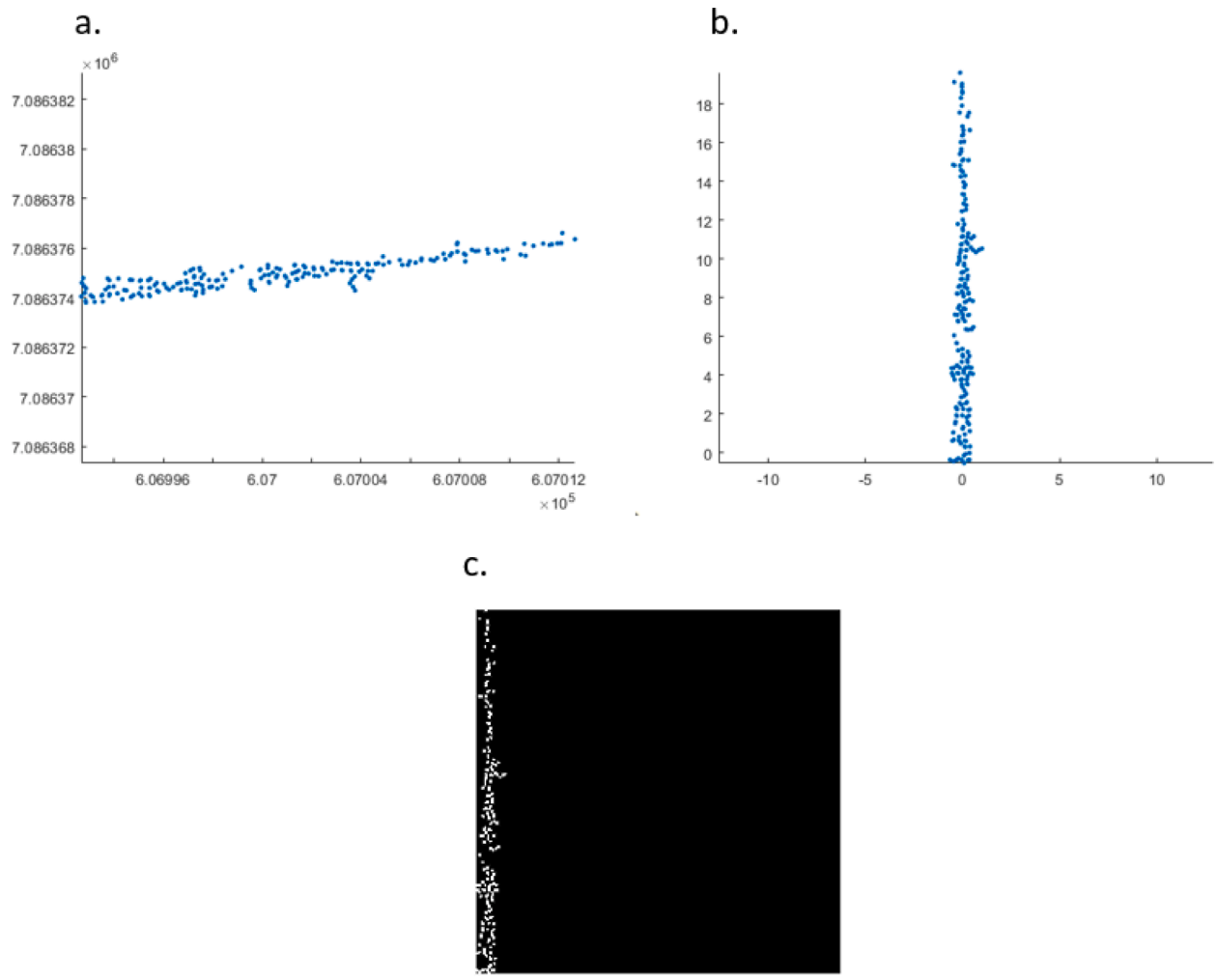

Fig. 4. Processing the fallen tree segments for classification. a) The original point cloud representation of a fallen tree segment. b) The rotated point cloud representation. c) A binary image of the fallen tree segment scaled and padded to the size of the required CNN input size.

and point cloud representation extraction (Section 2.7) algorithms on these point clouds, and labeling the detected and delineated fallen tree segments manually using visual inspection. None of the 100 test sites intersected with the 103 sample plots from which the reference data were collected.

Several pretrained CNNs were tuned and evaluated, including AlexNet (Krizhevsky et al., 2012), GoogLeNet (Szegedy et al., 2015), Inception-v3 (Szegedy et al., 2016), ResNet-18 (He et al., 2016), ResNet-50 (He et al., 2016), VGG16 (Simonyan & Zisserman, 2014) and VGG19 (Simonyan & Zisserman, 2014). AlexNet was selected as the final network, as its classification accuracy was similar to the accuracies of the other networks, but its prediction time was the fastest.

2.9. Validation

2.9.1. Tree detection

The performance of the fallen tree detection method was validated by running the method on the 103 sample plots and comparing the detected fallen tree segments to the reference data. The line representations of the fallen tree segments were manually matched with the line representations of reference trees (Fig. 5). A reference tree was determined as detected if the horizontal distance to the closest line segment was less than 1 m and the difference in orientation between the line segment and reference tree was less than 10°. Furthermore, the matched line segment needed to cover at least 30% of the length of the reference tree. If several line segments had been formed of one reference tree, they were counted as a single match of the tree.

The metrics used for measuring the performance of the detection method were precision (Eq. (1)) and recall (Eq. (2)). Precision measures the share of line segments that represent field measured reference trees, whereas recall represents the share of reference trees that were detected. The equations for precision and recall are the following:

$$Precision = \frac{TP}{TP + FP} \quad (1)$$

$$Recall = \frac{TP}{TP + FN} \quad (2)$$

In Eq. (1) and Eq. (2), *TP* denotes the number of true positives (i.e., the number of line segments that were matched with a reference tree), *FP* denotes the number of false positives (i.e., the number of line segments that were not matched with a reference tree), and *FN* denotes the number of false negatives (i.e., the number of reference trees for which a matching line segment was not found).

In addition to the overall metrics, the metrics were calculated separately for plots located in old-growth forests and managed forests. This allowed inspecting how the performance of the detection method differs in these two types of forest. Furthermore, the recall metric was calculated for different reference tree species, lengths, diameters, volumes, and decay classes to inspect how the performance of the detection method varies between different types of fallen trees. Moreover, the differences between species-specific recalls were tested using Fisher's

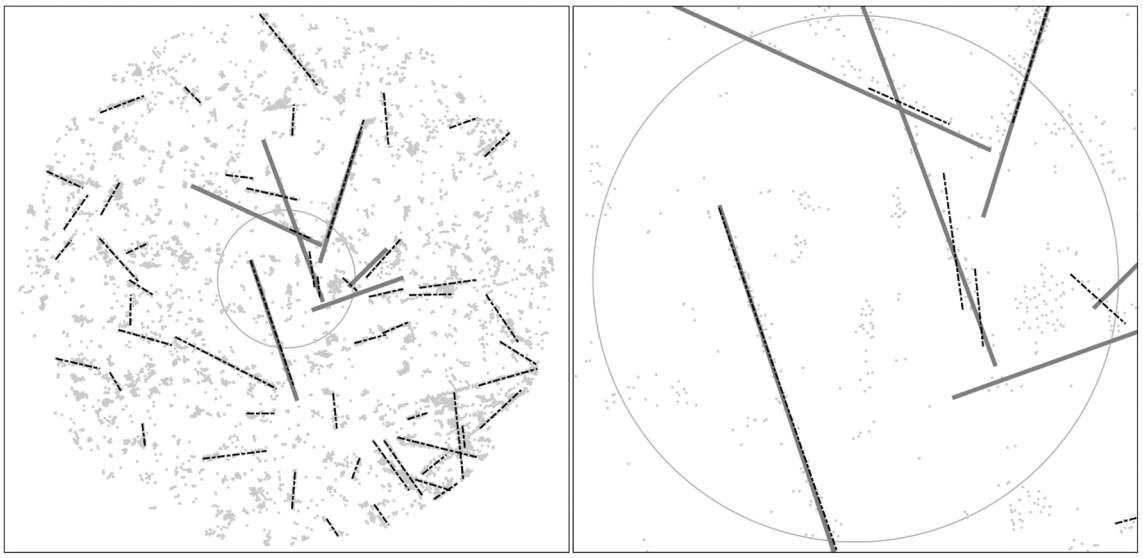

Fig. 5. Manual matching on one sample plot. The image on the left shows the whole area on which fallen tree detection was applied, whereas the image on the right shows a close-up view of the sample plot. The light gray dots are ALS data, the solid lines are reference trees, and the dashed/dotted lines are line segments detected with the iterative Hough transform based method presented in Section 2.6. In this case, two reference trees were matched with a line segment. Note that the circle in the center of the images represents the sample plot boundary. The iterative Hough transform based method was applied to the area within 35 m from the sample plot center, as this ensured that even the longest reference trees falling partially outside the sample plot were visible in full in the point cloud. The figure on the left shows a large number of line segments that were not matched with a reference tree, as no reference tree data were available outside the sample plot. However, only the non-matched line segments located fully or partially within the sample plot were calculated as false positives.

(1922) exact test to examine whether the differences in recall were statistically significant. Precision was not calculated for the different reference tree types, as, for example, determining the tree species of the fallen tree segments not matched with a reference tree was not possible.

2.9.2. Impact of vegetation structure

The impact of the surrounding vegetation structure on the performance of the fallen tree detection method was examined by fitting binomial regression models to plot-level observations. Each fitted model has one stand characteristic (Appendix B) as the independent variable and one performance metric (precision or recall) as the dependent variable.

The performance metrics follow a binomial distribution

$$\Pr(X = k) = \binom{n}{k} p^k (1-p)^{n-k} \tag{3}$$

where X is a random variable, n is the number of trials, k is the number of successful trials and p is the probability of success – the parameter of the binomial distribution. When modelling precision, n is the number of line segments, k is the number of line segments that were matched with a reference tree and p is the precision estimate. When modelling recall, n is the number of reference trees, k is the number of reference trees matched with a line segment and p is the recall estimate.

In binomial regression, the objective is to find the coefficients β_0 and β_1 that can be used to predict the parameter of the binomial distribution, p, given the value of an independent variable (x). As p is bounded between 0 and 1, a link function is needed to restrict the possible values of p that can be predicted. When using the logit link function, the relationship between the dependent variable p and independent variable x is

$$logit(p) = \log\left(\frac{p}{1-p}\right) = \beta_0 + \beta_1 x \tag{4}$$

Given the plot-level observations of line segments, reference trees and stand characteristics, the best-fit coefficients β_0 and β_1 can be found by maximizing the likelihood function

$$L = \prod_{i=1}^{N} \binom{n_i}{k_i} p_i^{k_i} (1-p_i)^{n_i - k_i} \tag{5}$$

where n_i is the number of trials on plot i, k_i is the number of successful trials on plot i and p_i is the observed parameter (precision/recall) for plot i. Once the best-fit coefficients have been found, the predicted value for precision/recall can be acquired using eq. (6):

$$\hat{p}_i = \frac{1}{1 + \exp(-(\beta_0 + \beta_1 x_i))}, \tag{6}$$

where $\hat{p}_i$ is the predicted precision/recall of sample plot i, β_0 and β_1 are the best-fit coefficients and x_i is the stand characteristic value of sample plot i.

Each fitted binomial regression model was evaluated using McFadden's (1977) R-squared. This allowed inspecting the strength of the relationship between each stand characteristic and the performance metrics of the detection method. McFadden's R-squared, or likelihood ratio index, is a pseudo R-squared measure that is used for estimating the goodness-of fit of logistic regression models. Thus, it is logistic regression's equivalent for the ordinary R-squared value used in linear regression. McFadden's R-squared is defined as:

$$R^2 = 1 - \frac{\ln(L_{model})}{\ln(L_{null})}, \tag{7}$$

where L_{model} is the likelihood of the fitted model and L_{null} is the likelihood of a null model (i.e., the model that only includes an intercept). McFadden's R-squared ranges between 0 and 1, as does the ordinary R-squared. However, the values of these two measures are not directly comparable.

The significance of McFadden's R-squared can be tested by calculating the deviance statistic:

$$D = 2(\ln(L_{model}) - \ln(L_{null})) \tag{8}$$

This deviance statistic has a Chi-squared distribution with degrees of freedom equal to the difference between the degrees of freedom of the fitted model and the null model. Thus, when using a 95% confidence

interval, the fitted model differs significantly from the null model if the p-value of the deviance statistic is smaller than 0.05.

3. Results

3.1. Performance of the fallen tree detection method

3.1.1. Performance by fallen tree type

The recall and precision calculated using all reference trees were 0.30 and 0.31, respectively. This means that the detection method was able to detect 30% of the reference trees, whereas 31% of the detected fallen tree segments could be matched with reference trees. However, recall was clearly positively correlated with the size (length, diameter and volume) of fallen trees, as indicated by Fig. 6. When inspecting only reference trees longer than or equal to 20 m, the recall increased from the original 30% to 75% (Fig. 6a). Similarly, the method detected 78% of reference trees with a diameter equal to or above 300 mm, as opposed to the 30% detected when using the original diameter threshold of 100 mm (Fig. 6b). The same positive trend is evident in the volume-based recalls (Fig. 6c). In contrast to tree size, decay class correlated negatively with recall (Fig. 6d), indicating that heavily decayed trees were less likely to be detected than more recently downed trees. However, the impact of decay state was significantly lower than the impact of tree size.

Table 4 shows that there were some differences between the recall of different reference tree species. The recall of aspen was the highest (0.50), but the number of reference aspens was only four and thus Fisher's test indicated a statistically insignificant difference between the recall of aspen and the recalls of the other three species. Furthermore, the mean diameter of reference aspens likely had a positive impact on recall, as it was significantly larger than the mean diameters of other species (Table 1). The recalls of the two coniferous species (pine 0.24, spruce 0.36) were somewhat higher than the recall of birch (0.16), although only the difference between the recalls of spruce and birch was statistically significant.

Table 4
Recall by tree species.

Species	Recall	True positives	False negatives
Scots pine	0.24	20	64
Norway spruce	0.36	54	94
Silver birch and downy birch	0.16	6	31
European aspen	0.50	2	2

3.1.2. Performance in managed and old-growth forests

Table 5 shows the performance of the detection method calculated separately for the 17 sample plots located in managed forests and the 86 sample plots located in old-growth forests. Both precision and recall were very low in managed forests. In fact, the method detected only one out of the 27 reference trees located in managed forest plots and created many false tree detections. In contrast, precision and recall were significantly higher in old-growth forests. The method detected 34% of all reference trees located in old-growth forests and 36% of the fallen tree segments generated by the method were true detections.

Table 5
The performance of the detection method in managed and old-growth forests. TP, FP and FN denote the numbers of true positives, false positives, and false negatives, respectively.

	Managed forest	Old-growth forest
Precision	0.02	0.36
Recall	0.04	0.34
TP	1	80
FP	44	142
FN	27	156

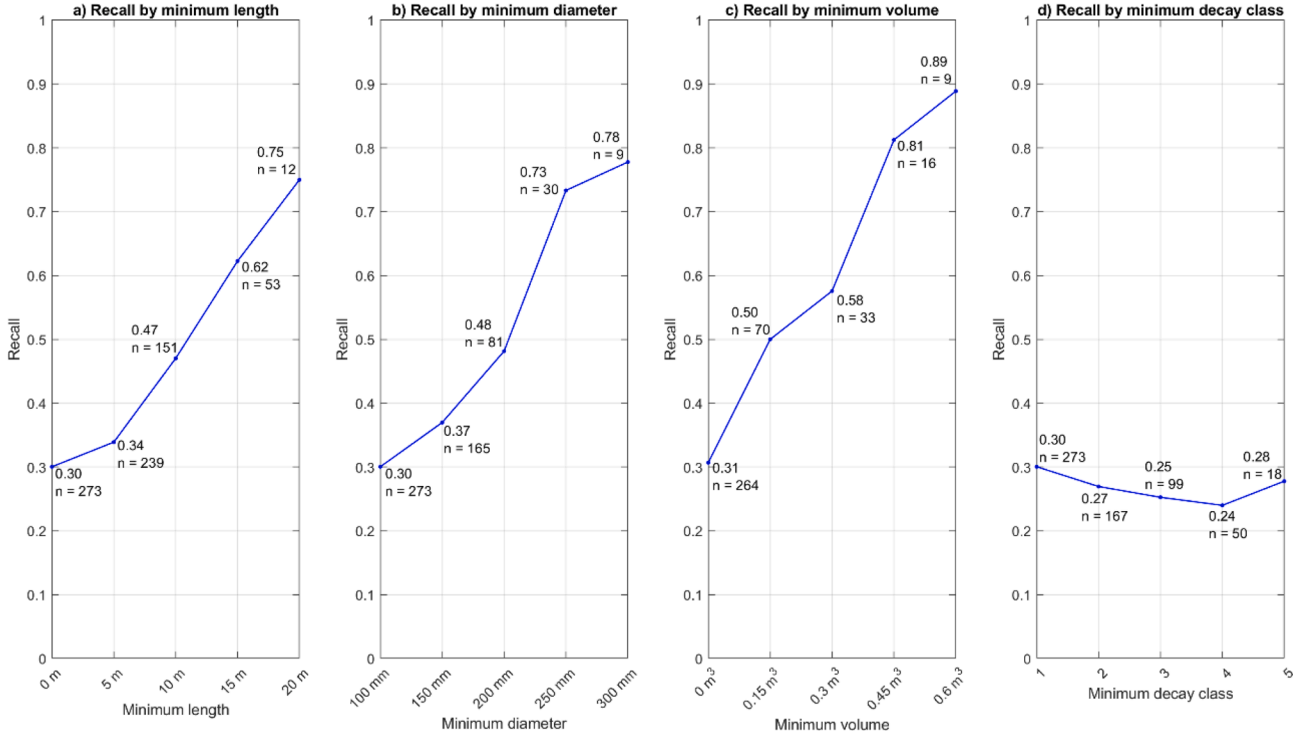

Fig. 6. Recalls by different fallen tree characteristics. a) Recall by minimum length. b) Recall by minimum diameter. c) Recall by minimum volume. d) Recall by minimum state of decay. The decay classes are presented in Appendix A. N denotes the number of observations. Each figure shows the recalls calculated using five different minimum values for the fallen tree characteristics. For example, the third data point in a) shows that the method detected 47% of reference trees with a length equal to or above 10 m.

3.2. Impact of vegetation structure

The impact of vegetation structure on the performance of fallen tree detection was examined by inspecting the relationship between stand characteristics (Appendix B) and performance metrics (precision and recall) calculated at the sample-plot level. Fig. 7, Fig. 8 and Fig. 9 present binomial regression models fit to plot-level observations. The stand characteristics are used as independent variables and the metrics describing the performance of the detection algorithm (precision and recall) are used as dependent variables. Each of the binomial regression curves shows the dependency between one stand characteristic and performance metric. Note that the presented McFadden's R-squared values are not comparable between the precision and recall models, as the observations of the dependent variable are different, which affects the likelihoods on which McFadden's R-squared is based. However, the McFadden's R-squared values are comparable between the models with the same dependent variable.

Most measured stand characteristics had a positive correlation with the performance of the detection method. Tree size related characteristics (diameter, height and volume) were positively correlated with both the precision and recall of the method (Fig. 7 and Fig. 8). In addition, basal area and canopy cover correlated positively with precision (Fig. 7 and Fig. 8). In contrast, the correlation between precision and the amount of undergrowth was negative (Fig. 7). The performance of the detection method was most significantly affected by spruce-related stand characteristics, indicating that the method performs differently in spruce-dominant areas compared to pine and birch-dominant areas. In fact, the height and diameter of spruces were the only species-specific stand characteristics with a statistically significant impact on recall.

4. Discussion

The objective of this study was to develop and test an automated ALS-based fallen tree detection method and evaluate the impact of fallen tree and vegetation structure -related factors on its performance. The method was developed for ALS point clouds with low to moderate point densities and thus the approach relies on simple line detection. The method was able to detect 30% of the 273 reference trees (minimum diameter 100 mm) with a precision of 31%. The fallen tree detection process included several parameters, most of which were described in Section 2.6. The values of these parameters were selected based on experiments, although a systematic sensitivity analysis was not performed. Thus, the results of this study could be slightly different if a more systematic approach for selecting the parameter values had been included in the study.

4.1. Impact of fallen tree characteristics

The various characteristics of the reference trees affected their detection. Firstly, the size of reference trees had a significant impact on their detection. The probability of detecting a large tree (length-, diameter-, and volume-wise) was higher than the probability of detecting a small tree. This result is rather fortunate, as, from an ecological perspective, large trees are more valuable than small trees (Andersson and Hytteborn, 1991; Bader et al. 1995). The higher detection rate of large trees is an intuitive result, as larger objects stand out from their surroundings better than smaller objects. From a more technical perspective, a large tree generates plenty of laser returns, which increases the possibility of a line being detected in the location of the tree. Mücke et al. (2013), Nyström et al. (2014), and Polewski et al. (2015) reported similar observations regarding the relationship between fallen tree size and probability of detection. Secondly, the detection probability decreased as the state of decay increased. This result is also rather expected, as heavily decayed trees lie very close to the ground and are often covered by ground vegetation. A similar observation was reported by Mücke et al. (2013). Thirdly, there were some differences in the detection probability of the four different reference tree species. The

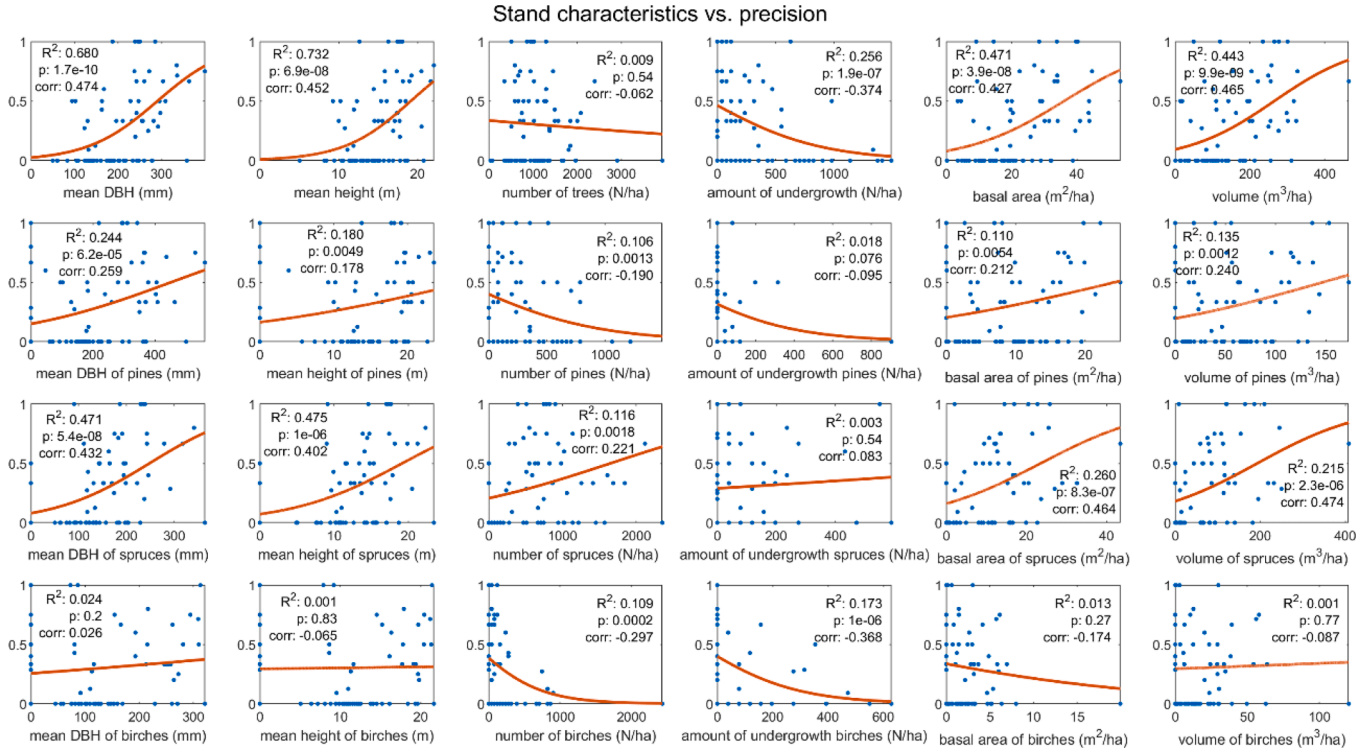

Fig. 7. Binomial regression plots of stand characteristics versus the precision of the fallen tree detection algorithm at different sample plots. R^2 is the McFadden's pseudo R-squared value that describes the strength of the relationship between the independent and dependent variable. P is the p-value of the deviance test that tests whether the model differs significantly from the null model. Refer to Appendix B for a more detailed description of the stand characteristics.

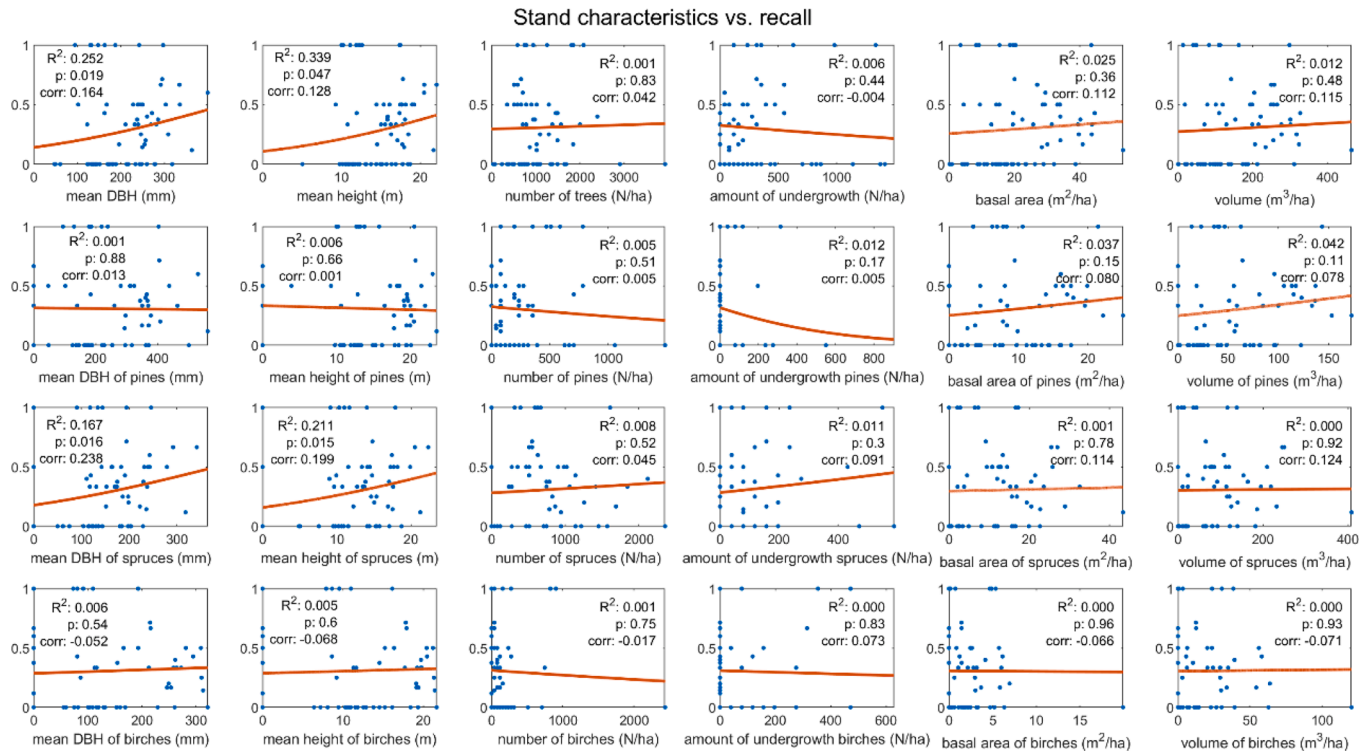

Fig. 8. Binomial regression plots of stand characteristics versus the recall of the fallen tree detection algorithm at different sample plots. R^2 is the McFadden's pseudo R-squared value that describes the strength of the relationship between the independent and dependent variable. P is the p-value of the deviance test that tests whether the model differs significantly from the null model. Refer to Appendix B for a more detailed description of the stand characteristics.

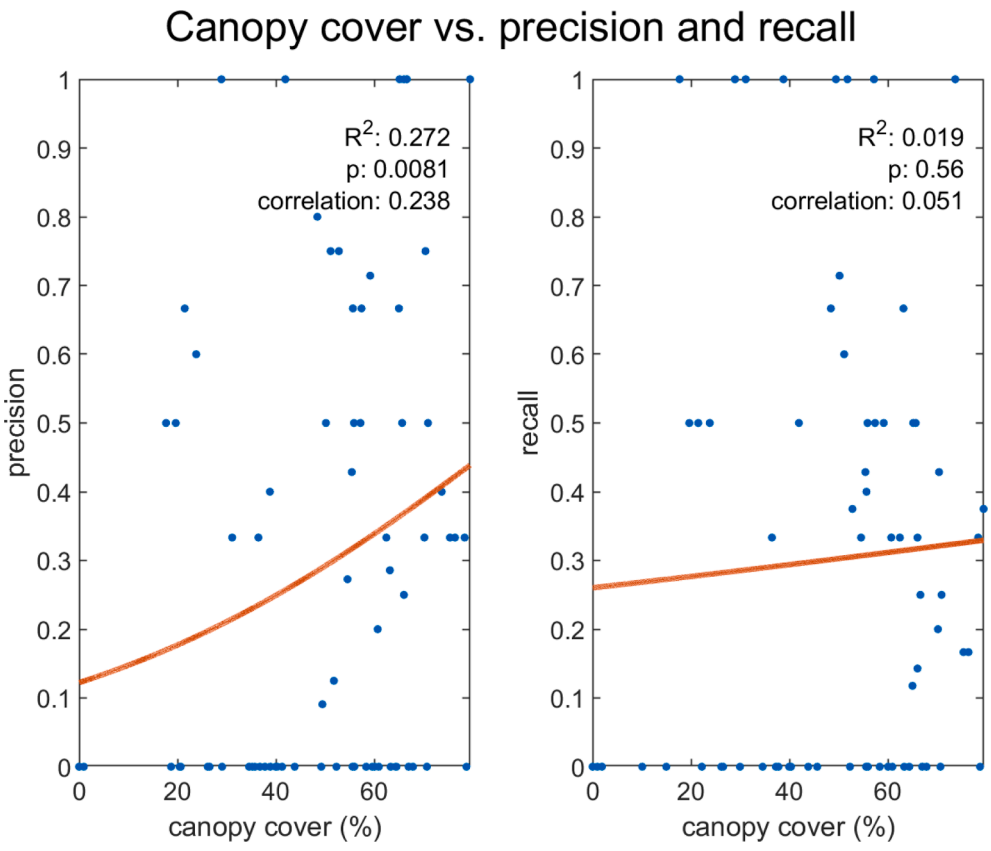

Fig. 9. Binomial regression plots of canopy cover versus precision (left) and recall (right). R^2 is the McFadden's pseudo R-squared value that describes the strength of the relationship between the independent and dependent variable. P is the p-value of the deviance test that tests whether the model differs significantly from the null model.

largest recall of aspen is likely explained by the large size and small number of reference aspens (Table 1), but the lower recall of birch compared to the two coniferous species cannot be explained by the difference in reference tree sizes. Nyström et al. (2014) also reported a higher recall for coniferous than deciduous species and suggested that the small number of branches explained the high recall of pine. The same reason might be valid in our study as well. A large number of branches might result in laser pulses being reflected from the branches of the fallen tree rather than the trunk itself, which, in turn, decreases the possibility of the fallen tree being detected, especially if the detection method is based on detecting lines. Another reason for the lower recall of fallen birches might be related to the vegetation structure of the forest stands within which they are located. As Appendix D shows, the amount of undergrowth increases as the number and basal area of living birches increases, which, in turn, has a negative impact on the detection of fallen trees. The occurrences of living and fallen birches are related. Thus, the unfavorable vegetation structure of stands with significant amounts of birches indirectly impact the detection of fallen birches.

4.2. Impact of vegetation structure

In addition to the fallen tree characteristics, the detection of fallen trees was impacted by various characteristics of the forest stands in which they reside. Overall, these characteristics seemed to have a larger impact on the precision than the recall of the detection method. This indicates that the characteristics affected the method's tendency to create false positives more than the method's probability of detecting a fallen tree.

The only stand characteristic with a notable negative correlation with precision was the amount of undergrowth, which likely impacts precision in two ways. Firstly, undergrowth generates laser returns from the same height range as fallen trees. The point cloud filtering step (Section 2.5) was developed for removing these points, but the performance of this procedure was not optimal. Thus, especially in areas with dense undergrowth, many false fallen tree points remained, and the iterative Hough line detection step (Section 2.6) falsely interpreted these as fallen trees. Secondly, a dense undergrowth results in less ground returns, which hinders the accurate classification of the ground. An accurate ground classification is a crucial step in fallen tree detection, as fallen trees lie close to the ground. Errors in ground classification result in ground points being classified as above-ground points, which, in turn, results in false detections of fallen trees. Furthermore, ground classification errors result in some laser points originating from fallen trees being classified as ground points, which, in turn, leads to some fallen trees not being detected. Blanchard et al. (2011) and Lindberg et al. (2013) reported similar observations of the impact of undergrowth on the number of false positives.

The positive correlation between the size of surrounding living trees and the performance of the detection method indicates that the method performs best on areas with large trees. As both recall and precision were affected, this means that a larger proportion of fallen trees are detected and a larger proportion of detected trees are true observations. A likely explanation for this result is the positive correlation between living and fallen tree size. Areas with large living trees often contain large fallen trees which are easy to detect. In addition, the amount of undergrowth decreases as the size of living trees increases (Appendix E), which has a positive impact on precision.

The spruce-specific stand characteristics seemed to have the largest impact on both the precision and recall of the detection method. One reason for this could be that spruce-dominant sample plots contained larger fallen trees compared to pine and birch-dominant plots (Table 3), which resulted in a larger number of true positives relative to the number of false positives and false negatives. Another reason is perhaps related to the distinctive branch and crown architecture ion of spruces. Spruces often have a larger proportion of branches on the lower parts of the trunk compared to pines and birches (Claesson et al., 2001; Tahvanainen & Forss 2008). Thus, small spruces have many branches located close to the ground. Similar to undergrowth, these branches create laser returns that are mistakenly interpreted as fallen trees. Furthermore, the branches cover some of the fallen trees, which results in these trees not being detected. As the spruce size grows, the trees have less branches close to the ground level, which reduces the problem.

The basal area of the two coniferous species had a different effect on the precision of the detection method compared to birch. An increase in the basal area of spruces or pines resulted in an increase in precision, whereas an increase in the basal area of birches resulted in a decrease in precision. One possible reason for this is that the higher amount of undergrowth on birch-populated stands (Appendix D) decreased precision. Another possible reason are the differences in the types of undergrowth and ground vegetation between coniferous and deciduous stands. Several studies have reported that coniferous stands tend to have a moss-dominant ground vegetation layer, whereas deciduous stands contain more grasses and herbs (e.g., Majasalmi and Rautiainen, 2020; Muukkonen and Mäkipää, 2006; Saetre et al., 1997). A moss-dominant ground vegetation layer leaves the fallen trees visible, whereas grasses and herbs cover the fallen trees and create additional laser returns from close to the ground.

The precision of the detection method correlated positively with canopy cover, whereas recall was not affected. An increase in canopy cover reduces the number of laser returns from below canopy, resulting in a sparser point cloud from close to the ground. When the parameters of Hough line detection (e.g., the stopping condition introduced in Section 2.6) remain unchanged, this reduces the number of detected lines. Lines representing true and false fallen tree observations should be reduced in the same proportion, leaving precision unaffected. However, the positive correlation between canopy cover and precision indicates that an increase in canopy cover has a larger impact on the number of false observations than the number of true observations. A possible explanation for this surprising result is that the calculated canopy cover percentages were distorted in some cases, as the percentages were determined from laser points above five meters from ground. Sample plots with similar canopy covers might have been very different in reality. For example, the calculated canopy cover percentage for young stands where the canopy is mostly below five meters from ground would be significantly lower than the true percentage. Thus, sample plots for which the calculated canopy cover was large were likely to consist of larger trees than the plots with low canopy cover. As tree size correlated positively with precision (Section 3.2), the sample plots with large trees and a high canopy cover had a higher precision than the sample plots with small trees and low canopy cover.

4.2.0.1. Performance in managed and old-growth forests

The performance of the detection method was substantially higher in old-growth forest plots compared to managed forest plots. This is likely a result of two phenomena. Firstly, the reference trees in old-growth forest plots were, on average, larger than the trees in managed forest plots (Table 2). Secondly, the stand characteristics in old-growth forests were more favorable for detection (Appendix C). The managed forest plots in this study were located in rather young stands and thus the size of living trees was smaller than the living tree size in old-growth forest plots. In addition, the basal area of old-growth forest plots was larger. Both tree size and basal area were found to correlate positively with the performance of the detection method. Furthermore, the amount of undergrowth was significantly larger in managed forests than in old-growth forests and this stand characteristic was found to have a negative correlation with the performance of the detection method. Another factor possibly impacting the precision of managed forest plots were logging residues. Similarly as undergrowth, they generate laser returns from close to the ground, which results in more false positives.

4.3. Comparison to earlier studies

The point density of the ALS data used in this study was lower than the densities used in most earlier studies discussing ALS-based fallen tree detection. Thus, the detection approach was somewhat simplified compared to other studies. The 2D line detection approach used in this study likely limited the detection of more complex-shaped fallen trees. Still, accounting for the differences in point densities, the performance of our method was competitive with the other methods.

The only earlier studies validated in a boreal forest (Lindberg et al., 2013; Nyström et al., 2014) used a significantly higher point density (65 points/m^2) compared to the point density used in this study (15 points/m^2). Taking the difference in point densities into account, the precision (31%) and recall (30%) reached with our method were surprisingly similar to the values reached by Lindberg et al. (2013) (precision = 32%, recall = 41%) and Nyström et al. (2014) (precision = 51%, recall = 38%), especially as the reference trees used in our study were smaller on average. The mean diameter and length of reference trees in this study were 176.3 mm and 10.7 m, whereas in Lindberg et al. (2013) and Nyström et al. (2014) the corresponding values were 226 mm and 17.6 m. The line template matching approach used by both earlier studies probably outperforms the direct line detection approach used in this study in the detection of discontinuous fallen trees. However, template matching restricts the line search to a fixed line length, which prevents uncovering the true fallen tree dimensions. Furthermore, a line template matching approach, in which the most suitable line positions are searched exhaustively, is likely less efficient than a direct line detection approach.

Other earlier ALS-based fallen tree detection methods have been validated in somewhat different sites than the method used in this study. Mücke et al. (2013) reached a precision of 90% and a recall of 76% in a stand characterized as Euro-Siberian steppic woods. Their dataset was a full-waveform ALS dataset with a 29.4 points/m^2 density. Mücke et al. (2013) used a minimum diameter of 300 mm for reference trees. Our method detected 78% of reference trees with the same minimum diameter, which is almost exactly the same as the value reached by Mücke et al. (2013). However, the precision of our method was significantly lower, although the precisions are not directly comparable, as the parameters of our method were tuned to detect trees with a diameter equal to or above 100 mm. The reason for the very high precision of Mücke et al. (2013) is possibly that they used echo width information from the full-waveform data for filtering points located close to the ground. Echo width is related to surface roughness, which allows distinguishing the rather smooth surfaces of fallen trees from rougher surfaces, such as undergrowth and ground vegetation.

Polewski et al. (2015 & 2018) reported precisions ranging between 47% and 97% and recalls ranging between 34% and 71% for their detection method validated on five test plots located in the mountain mixed forest zone. They used ALS data with a 30 points/m^2 density. Their results were likely improved by the filtering step in which they visually examined the data and removed reference trees that were not visible in the point cloud as well as laser points representing fallen trees that were not included in the reference data. Polewski et al. (2015 & 2018) reported that their method is suitable for detecting fallen trees even in rather complex situations where a group of trees lie on top of each other, as the method was trained using simulated fallen tree data. However, the 3D shape contexts they used for classifying fallen tree segments require a sufficient number of laser points in order to be representative. It is unclear, whether a point cloud with a density significantly lower than 30 points/m^2 would suffice for 3D shape contexts.

The only earlier study with a lower point density than the one used in this study was conducted by Blanchard et al. (2011), who detected fallen trees in a burnt study site with very low canopy cover. They reached a recall of 73% using ALS data with a 10.5 points/m^2 density. The precision of the method was not mentioned. Blanchard et al. (2011) selected the reference trunks visually from the ALS data and orthophotos, which, similarly to the visual filtering step used by Polewski et al. (2015 & 2018), likely improved the results, as it ensured that the reference trunks were visible in the point cloud. The raster-based segmentation approach used by Blanchard et al. (2011) worked rather well for their relatively large reference trees (diameter 250–1500 mm, length 5–30 m). However, the coarse cell size of 0.5 m precludes the detection of smaller trees, which is not the case with a method operating directly on the point cloud.

In general, the fallen tree detection method should be chosen based on the application and the data available. Complex multiphase methods, such as the one presented by Polewski et al. (2015 & 2018) allow detecting fallen trees in more complex scenarios but require a higher point density. In contrast, simpler approaches, such as the one presented in this study, should be used for point clouds with lower point densities. An additional benefit of such methods is that their computational cost is lower, which allows using the methods for larger datasets. Fallen tree detection, and object detection in general, always includes a tradeoff between precision and recall. The tradeoff should be considered when selecting the most suitable detection method and tuning the parameters of the method. The biggest problem with our method was its tendency to generate false positives, especially on complex stands with a large amount of undergrowth and ground vegetation. This tendency was amplified by the fact that the parameters of the detection method were selected to favor recall over precision, as the reference trees were, on average, rather small. The generation of false positives could be reduced by improving the performance of the point cloud filtering step (Section 2.5). The point feature histograms used by Polewski et al. (2015 & 2018) or the echo width information used by Mücke et al. (2013) could be useful. Echo width information would, however, require full-waveform data.

5. Conclusions

This study showed that fallen trees can be mapped using ALS data with a moderate point density, indicating that automated large-scale mapping of dead wood could be possible in the near future. However, whether the mapping accuracy using such ALS data is sufficient, depends largely on the application and characteristics of the site of interest. An application requiring accurate tree-level information of even the smallest trees would certainly require a significantly higher point density than the one used in this study. In contrast, a point density around 15 points/m^2 would suffice for an application requiring only indicative fallen tree information or information from the largest fallen tree trunks.

The detection method presented in this study included several parameters that could be tuned to best suit the target from which fallen trees are to be detected. The parameter values used in this study were selected based on non-systematic experimenting. Thus, the systematic selection of optimal parameter values could be an interesting topic for further research.

In addition to detecting fallen trees, the method presented in this study delineated the detected trees from the point cloud. The point cloud representations of fallen trees could potentially be used for estimating the characteristics (e.g., volume and dimensions) of the fallen trees. Dead wood volume information originating from fallen trees would be beneficial for many biodiversity-related applications. Thus, further research should focus on how characteristics can be estimated from the point cloud representations of fallen trees.

The results of this study showed that the characteristics of fallen trees have a significant effect on how well they are detected. Large trees are detected with a high rate, whereas the detection rate of smaller trees is lower. Fortunately, from an ecological perspective, large trees are more important. In addition to fallen tree characteristics, the characteristics of the surrounding vegetation affect the detection accuracy. Fallen tree detection performs best in areas with large living trees, and a low amount of undergrowth and ground vegetation, such as boreal old-

growth forests or mature managed stands. In contrast, young stands with small trees and a dense undergrowth are challenging environments for the detection of fallen trees. Thus, with the current point densities used in large-scale laser scanning campaigns, tree-level information acquisition is most suitable for undisturbed natural forests and mature managed forest stands.

CRediT authorship contribution statement

Einari Heinaro: Conceptualization, Methodology, Software, Validation, Formal analysis, Investigation, Data curation, Writing - original draft, Writing - review & editing, Visualization, Funding acquisition. **Topi Tanhuanpää:** Conceptualization, Methodology, Validation, Writing - review & editing, Supervision, Project administration, Funding acquisition. **Tuomas Yrttimaa:** Conceptualization, Methodology, Software, Writing - review & editing. **Markus Holopainen:** Conceptualization, Resources, Writing - review & editing, Project administration, Funding acquisition. **Mikko Vastaranta:** Conceptualization, Writing - review & editing, Project administration, Funding acquisition.

Declaration of Competing Interest

The authors declare that they have no known competing financial interests or personal relationships that could have appeared to influence the work reported in this paper.

Acknowledgements

The authors would like to thank Mr. Osmo Suominen for helping with field data collection and M Sc. Ninni Mikkonen for providing motivational insights for conducting the research. Furthermore, the authors are grateful for the support provided by the Finnish Environment Institute (SYKE).

Funding

The study was funded by the LIFE financial instrument of the European Union (Beetles LIFE (LIFE17/NAT/FI/000181)), the Academy of Finland's Strategic Research Council (IBC-Carbon, project number 312559), the Academy of Finland's Flagship Program (UNITE, project number 337127) and the Doctoral Program in Sustainable Use of Renewable Natural Resources (AGFOREE) at the University of Helsinki.

Appendix A. . The classification used for describing the state of decay of fallen trees. The classification was adopted from the Finnish national forest inventory (Metsäntutkimuslaitos, 2009).

State of decay/decay class	Description
1	The wood is hard. When pushed into the wood, a knife penetrates the wood with only a few millimeters.
2	The wood is rather hard. When pushed into the wood, a knife penetrates the wood with 1–2 cm.
3	The wood is rather soft. When pushed into the wood, a knife penetrates the wood with 3–5 cm.
4	The wood is soft. The whole blade of a knife penetrates the wood.
5	The wood is very soft and falls apart when touched.

Appendix B. . Stand characteristics and their ranges on the sample plot level.

Stand characteristic	Explanation	Min	Med	Max
number of trees	Number of living trees with a DBH above 45 mm (N/ha)	0	786	3930
number of pines	Number of living pines with a DBH above 45 mm (N/ha)	0	236	1493
number of spruces	Number of living spruces with a DBH above 45 mm (N/ha)	0	275	2358
number of birches	Number of living birches with a DBH above 45 mm (N/ha)	0	39	2436
amount of undergrowth	Number of living trees with a DBH under 45 mm (undergrowth) (N/ha)	0	196	1493
amount of undergrowth pines	Number of living pines with a DBH below 45 mm (undergrowth) (N/ha)	0	0	904
amount of undergrowth spruces	Number of living spruces with a DBH below 45 mm (undergrowth) (N/ha)	0	39	589
amount of undergrowth birches	Number of living birches with a DBH below 45 mm (undergrowth) (N/ha)	0	0	629
basal area	Basal area (m^2/ha)	0	14.6	53.2
basal area of pines	Basal area of pines (m^2/ha)	0	6.9	25.0
basal area of spruces	Basal area of spruces (m^2/ha)	0	3.4	43.4
basal area of birches	Basal area of birches (m^2/ha)	0	0.7	19.9
volume	Tree volume (m^3/ha)	0	99.3	464.3
volume of pines	Volume of pines (m^3/ha)	0	39.5	172.7
volume of spruces	Volume of spruces (m^3/ha)	0	17.7	407.9
volume of birches	Volume of birches (m^3/ha)	0	4.3	120.3
mean height	Mean tree height weighted by basal area (Lorey's mean height) (m)	0	14.2	22.1
mean height of pines	Mean tree height of pines weighted by basal area (m)	0	12.9	23.6
mean height of spruces	Mean tree height of spruces weighted by basal area (m)	0	10.6	23.4
mean height of birches	Mean tree height of birches weighted by basal area (m)	0	9.4	21.6
mean DBH	Mean DBH weighted by basal area (mm)	0	184	399
mean DBH of pines	Mean DBH of pines weighted by basal area (mm)	0	182	561
mean DBH of spruces	Mean DBH of spruces weighted by basal area (mm)	0	122	364
mean DBH of birches	Mean DBH of birches weighted by basal area (mm)	0	82	321
canopy cover	Canopy cover (%) derived from ALS data	0	41.3	79.5

Appendix C. . Median stand characteristics in managed and old-growth forest.

	Managed forest	Old-growth forest
mean DBH (mm)	172.5	189.6
mean DBH of pines (mm)	181.6	182.9
mean DBH of spruces (mm)	94.7	132.4
mean DBH of birches (mm)	116.5	74.4
mean height (m)	13.1	14.5
mean height of pines (m)	13.0	12.8
mean height of spruces (m)	9.5	11.1
mean height of birches (m)	11.5	8.4
number of trees (N/ha)	510.9	805.6
number of pines (N/ha)	275.1	216.1
number of spruces (N/ha)	117.9	412.6
number of birches (N/ha)	157.2	39.3
amount of undergrowth (N/ha)	746.7	176.8
amount of undergrowth pines (N/ha)	0	0
amount of undergrowth spruces (N/ha)	39.3	39.3
amount of undergrowth birches (N/ha)	196.5	0
basal area (m^2/ha)	10.8	16.7
basal area of pines (m^2/ha)	7.1	6.5
basal area of spruces (m^2/ha)	0.9	7.3
basal area of birches (m^2/ha)	1.3	0.4
volume (m^3/ha)	60.8	107.9
volume of pines (m^3/ha)	40.6	33.4
volume of spruces (m^3/ha)	3.9	47.9
volume of birches (m^3/ha)	9.1	1.9
canopy cover (%)	37.3	45.6

Appendix D. . The relationship between stand characteristics and the amount of undergrowth calculated at the sample plot level. Relative basal area is the basal area of a specific species divided by the total basal area of the sample plot. Volumes were excluded from the plots, as they were derived from diameters and heights.

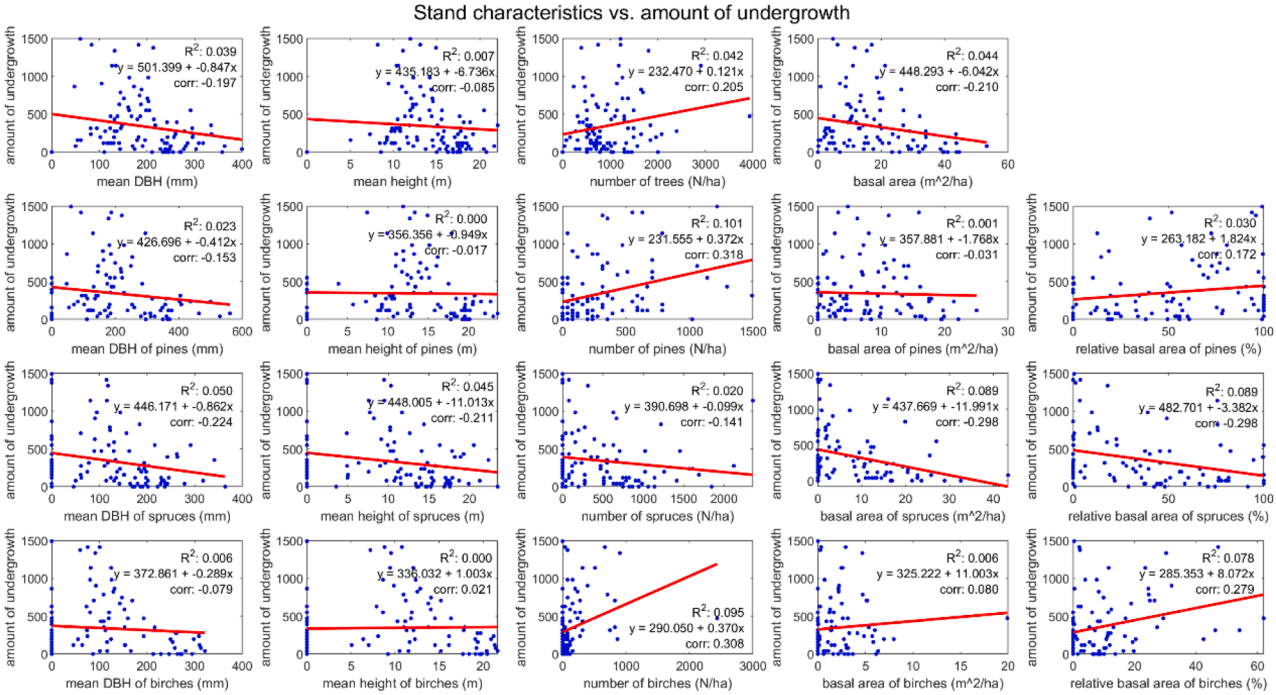

Appendix E. . Linear regression models showing the relationship between stand characteristics and the amount of undergrowth calculated at the sample plot level.

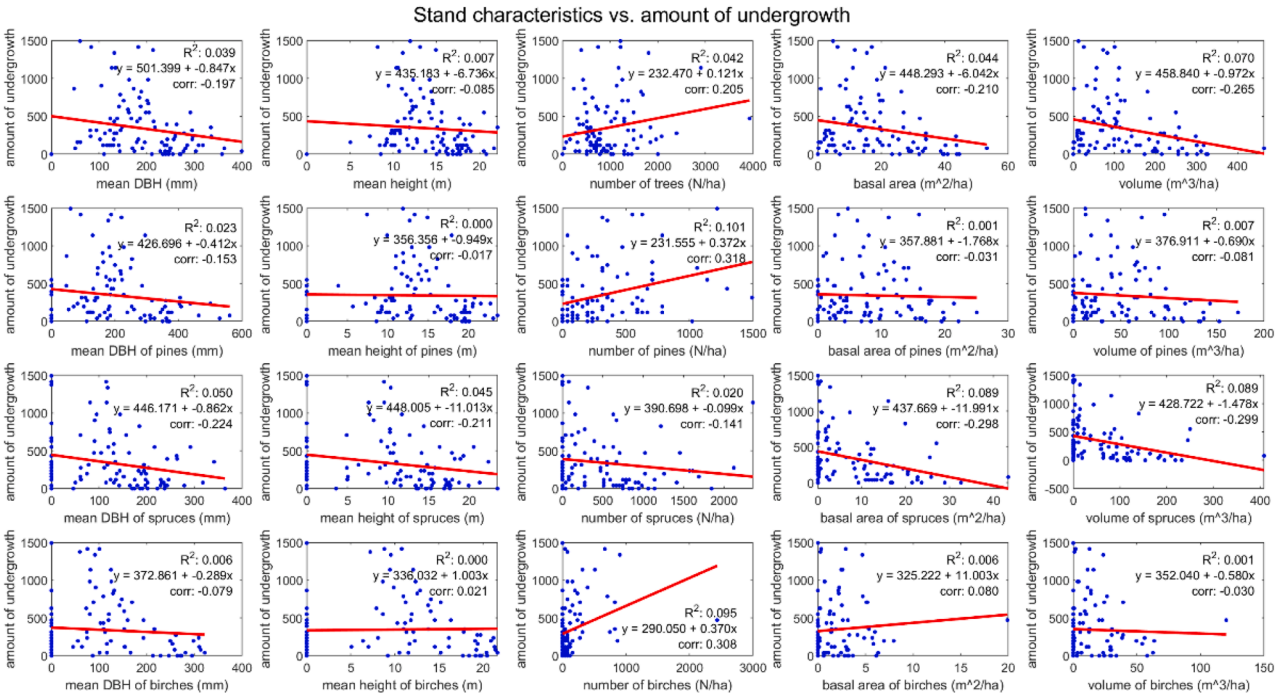

References

Andersson, L.I., Hytteborn, H., 1991. Bryophytes and decaying wood- a comparison between managed and natural forest. Ecography 14 (2), 121–130. https://doi.org/10.1111/j.1600-0587.1991.tb00642.x.

Axelsson, P., 2000. DEM Generation from Laser Scanner Data using Adaptive TIN Models. Int. Arch. Photogramm. Remote Sens. 33 (B4), 110–117.

Blanchard, S.D., Jakubowski, M.K., Kelly, M., 2011. Object-Based Image Analysis of Downed Logs in Disturbed Forested Landscapes Using Lidar. Remote Sens. 3 (11), 2420–2439. https://doi.org/10.3390/rs3112420.

Bader, P., Jansson, S., Jonsson, B.G., 1995. Wood-inhabiting fungi and substratum decline in selectively logged boreal spruce forests. Biol. Conserv. 72 (3), 355–362. https://doi.org/10.1016/0006-3207(94)00029-p.

Claesson, S., Sahlén, K., Lundmark, T., 2001. Functions for Biomass Estimation of Young Pinus sylvestris, Picea abies and Betula spp. from Stands in Northern Sweden with High Stand Densities. Scand. J. For. Res. 16 (2), 138–146. https://doi.org/10.1080/028275801300088206.

Dalitz, C., Schramke, T., Jeltsch, M., 2017. Iterative Hough Transform for Line Detection in 3D Point Clouds. Image Process. On Line 7, 184–196. https://doi.org/10.5201/ipol.2017.208.

Ducey, M.J., Williams, M.S., Gove, J.H., Roberge, S., Kenning, R.S., 2013. Distance-limited perpendicular distance sampling for coarse woody debris: theory and field results. Forestry 86 (1), 119–128. https://doi.org/10.1093/forestry/cps059.

Duda, R.O., Hart, P.E., 1972. Use of the Hough transformation to detect lines and curves in pictures. Commun. ACM 15 (1), 11–15. https://doi.org/10.1145/361237.361242.

Fisher, R.A., 1922. On the Interpretation of χ 2 from Contingency Tables, and the Calculation of P. J. R. Stat. Soc. 85 (1), 87. https://doi.org/10.2307/2340521.

Frome A., Huber D., Kolluri R., Bülow T., Malik J. (2004) Recognizing Objects in Range Data Using Regional Point Descriptors. In: Pajdla T., Matas J. (eds) Computer Vision - ECCV 2004. ECCV 2004. Lect. Notes Comput. Sci., vol 3023. Springer, Berlin, Heidelberg. https://doi.org/10.1007/978-3-540-24672-5_18.

Harmon, M.E., Franklin, J.F., Swanson, F.J., Sollins, P., Gregory, S.V., Lattin, J.D., Anderson, N.H., Cline, S.P., Aumen, N.G., Sedell, J.R., Lienkaemper, G.W., Cromack Jr., K., Cummins, K.W., 1986. Ecology of coarse woody debris in temperate ecosystems. Adv. Ecol. Res. 15, 133–302.

He, K., Zhang, X., Ren, S., Sun, J., 2016. Deep residual learning for image recognition. In: Proceedings of the IEEE Conference on Computer Vision and Pattern Recognition. pp. 770–778.

Heinaro, E., 2021a. Detection of individual fallen trees from airborne laser scanning data. Mendeley Data V1. https://doi.org/10.17632/hbhvgn8p7b.1.

Heinaro, E. (2021b). Fallen_tree_detection. Github.com. [Online]. Available: https://github.com/Eikka12/Fallen_tree_detection [Accessed 23.3.2021].

Hodgson, M.E., Bresnahan, P., 2004. Accuracy of Airborne Lidar-Derived Elevation. Photogramm. Eng. Remote Sens. 70 (3), 331–339. https://doi.org/10.14358/pers.70.3.331.

Hough, P. V. C. (1962). Method and means for recognizing complex patterns US Patent 3069654. Washington, DC: Patent and Trademark Office.

Jonsson, B.G., Kruys, N., Ranius, T., 2005. Ecology of species living on dead wood – lessons for dead wood management. Silva Fenn. 39 (2) https://doi.org/10.14214/sf.390.

Kangas, A., 2006. Sampling rare populations. In: Kangas, A., Maltamo, M. (Eds.), Managing Forest Ecosystems. Springer, Dordrecht, 10.1007/1-4020-4381-3_8.

Krizhevsky, A., Sutskever, I., Hinton, G.E., 2012. Imagenet classification with deep convolutional neural networks. In: In Advances in Neural Information Processing Systems, pp. 1097–1105.

Laasasenaho, J., 1982. Taper Curve and Volume Functions for Pine, Spruce and Birch. Commun. Inst. For. Fenn. 108, 1–74.

Lindberg, E., Hollaus, M., Mücke, W., Fransson, J., Pfeifer, N., 2013. Detection of lying tree stems from airborne laser scanning data using a line template matching algorithm. ISPRS Ann. Photogramm. Remote Sens. Spat. Inf. Sci. II-5/W2, 169–174. https://doi.org/10.5194/isprsannals-ii-5-w2-169-2013.

Majasalmi, T., Rautiainen, M., 2020. The impact of tree canopy structure on understory variation in a boreal forest. For. Ecol. Manag. 466, 118100 https://doi.org/10.1016/j.foreco.2020.118100.

McFadden, D., 1977. Quantitative methods for analyzing travel behavior of individuals: some recent developments. Cowles Found. Discuss. Pap. 474, 1–47.

Metsäntutkimuslaitos, 2009. VMI11. Metla.fi. [Online]. Available: http://www.metla.fi/ohjelma/vmi/vmi11-maasto-ohje09-2p.pdf [Accessed 20.5.2019] (In Finnish).

Miura, N., Jones, S.D., 2010. Characterizing forest ecological structure using pulse types and heights of airborne laser scanning. Remote Sens. Environ. 114 (5), 1069–1076. https://doi.org/10.1016/j.rse.2009.12.017.

Mücke, W., Deák, B., Schroiff, A., Hollaus, M., Pfeifer, N., 2013. Detection of fallen trees in forested areas using small footprint airborne laser scanning data. Can. J. Remote Sens. 39 (sup1), S32–S40. https://doi.org/10.5589/m13-013.

Muukkonen, P., Mäkipää, R., 2006. Empirical biomass models of understorey vegetation in boreal forests according to stand and site attributes. Boreal Environ. Res. 11, 355–369.

Nyström, M., Holmgren, J., Fransson, J.E., Olsson, H., 2014. Detection of windthrown trees using airborne laser scanning. Int. J. Appl. Earth Obs. Geoinf. 30, 21–29. https://doi.org/10.1016/j.jag.2014.01.012.

Näslund, M. (1936). Skogsförsöksanstaltens gallringsförsök i tallskog. Meddelanden från Statens Skogsförsöksanstalt, 29. (In Swedish).

Pesonen, A., Maltamo, M., Eerikäinen, K., Packalèn, P., 2008. Airborne laser scanning-based prediction of coarse woody debris volumes in a conservation area. For. Ecol. Manag. 255 (8–9), 3288–3296. https://doi.org/10.1016/j.foreco.2008.02.017.

Pesonen, A., Kangas, A., Maltamo, M., Packalén, P., 2010a. Effects of auxiliary data source and inventory unit size on the efficiency of sample-based coarse woody debris inventory. For. Ecol. Manag. 259 (10), 1890–1899. https://doi.org/10.1016/j.foreco.2010.02.001.

Pesonen, A., Maltamo, M., Kangas, A., 2010b. The comparison of airborne laser scanning-based probability layers as auxiliary information for assessing coarse woody debris.

Int. J. Remote Sens. 31 (5), 1245–1259. https://doi.org/10.1080/01431160903380607.
Polewski, P., Yao, W., Heurich, M., Krzystek, P., Stilla, U., 2015. Detection of fallen trees in ALS point clouds using a Normalized Cut approach trained by simulation. ISPRS J. Photogramm. Remote Sens. 105, 252–271. https://doi.org/10.1016/j.isprsjprs.2015.01.010.
Polewski, P., Yao, W., Heurich, M., Krzystek, P., Stilla, U., 2018. Learning a constrained conditional random field for enhanced segmentation of fallen trees in ALS point clouds. ISPRS J. Photogramm. Remote Sens. 140, 33–44. https://doi.org/10.1016/j.isprsjprs.2017.04.001.
Rusu, R., Marton, Z., Blodow, N., Beetz, 2008. Learning informative point classes for the acquisition of object model maps. In: 10th International Conference on Control, Automation, Robotics and Vision, (pp. 643–650).
Saetre, P., Saetre, L., Brandtberg, P., Lundkvist, H., Bengtsson, J., 1997. Ground vegetation composition and heterogeneity in pure Norway spruce and mixed Norway spruce - birch stands. Can. J. For. Res. 27 (12), 2034–2042. https://doi.org/10.1139/x97-177.
Secretariat of the Convention on Biological Diversity. (2005). Handbook of the Convention on Biological Diversity, 3rd edition. Montreal, Canada.
Secretariat of the Convention on Biological Diversity. (2020). Global Biodiversity Outlook 5. Montreal, Canada.
Shi, J., Malik, J., 2000. Normalized cuts and image segmentation. IEEE Trans. Pattern Anal. Mach. Intell. 22 (8), 888–905.
Simonyan, K., & Zisserman, A. (2014). Very deep convolutional networks for large-scale image recognition. arXiv preprint arXiv:1409.1556.
Stokland, J.N., Siitonen, J., Jonsson, B.G., 2012. Biodiversity in dead wood. Cambridge University Press.
Ståhl, G., Ringvall, A., Fridman, J., 2001. Assessment of coarse woody debris: a methodological overview. Ecol. Bull. 57–70.
Ståhl, G., Gove, J., Williams, M., Ducey, M., 2010. Critical length sampling: a method to estimate the volume of downed coarse woody debris. Eur. J. For. Res. 129 (6), 993–1000. https://doi.org/10.1007/s10342-010-0382-3.
Su, J., Bork, E., 2006. Influence of Vegetation, Slope, and Lidar Sampling Angle on DEM Accuracy. Photogramm. Eng. Remote Sens. 72 (11), 1265–1274. https://doi.org/10.14358/pers.72.11.1265.
Szegedy, C., Liu, W., Jia, Y., Sermanet, P., Reed, S., Anguelov, D., Erhan, D., Vanhoucke, V., Rabinovich, A., 2015. Going deeper with convolutions. In: Proceedings of the IEEE conference on computer vision and pattern recognition, pp. 1–9.
Szegedy, C., Vanhoucke, V., Ioffe, S., Shlens, J., Wojna, Z., 2016. Rethinking the inception architecture for computer vision. In: Proceedings of the IEEE conference on computer vision and pattern recognition, pp. 2818–2826.
Tahvanainen, T., Forss, E., 2008. Individual tree models for the crown biomass distribution of Scots pine, Norway spruce and birch in Finland. For. Ecol. Manag. 255 (3–4), 455–467. https://doi.org/10.1016/j.foreco.2007.09.035.
Yrttimaa, T., Saarinen, N., Luoma, V., Tanhuanpää, T., Kankare, V., Liang, X., et al., 2019. Detecting and characterizing downed dead wood using terrestrial laser scanning. ISPRS J. Photogramm. Remote Sens. 151, 76–90. https://doi.org/10.1016/j.isprsjprs.2019.03.007.